4-27-2019

Adaptive and Supertwisting Adaptive Spacecraft Orbit Control Around Asteroids

Keum W. Lee
Catholic Kwandong University, kwlee@cku.ac.kr

Sahjendra N. Singh
University of Nevada, Las Vegas, sahjendra.singh@unlv.edu

Repository Citation

Lee, K. W., Singh, S. N. (2019). Adaptive and Supertwisting Adaptive Spacecraft Orbit Control Around Asteroids. *Journal of Aerospace Engineering, 32*(4), 1-14.
http://dx.doi.org/10.1061/(ASCE)AS.1943-5525.0001043

Adaptive and Super-Twisting Adaptive Spacecraft Orbit Control Around Asteroids

Keum W. Lee* and Sahjendra N. Singh†

Revised: November 18, 2017; and December 6, 2018; February 5, 2019

Abstract

The development of control systems for the orbit control of spacecraft around irregularly shaped rotating asteroids with uncertain parameters is the subject of this paper. The objective is to steer the spacecraft along prescribed orbits. In this study, first, a nonlinear adaptive law for orbit control is designed. This is followed by the design of a super-twisting adaptive (STWA) control system. In the closed-loop system, which includes the adaptive law or the STWA law, all the signals remain bounded, and the trajectory tracking error asymptotically converges to zero for any initial condition. Finally, under the assumption of boundedness of the derivative of the uncertain functions of the model in a region of the state space, a super-twisting control (STW) law for finite-time convergence of the trajectory is obtained. Based on the Lyapunov theory, stability properties of the closed-loop systems are analyzed. Simulation results for Eros 433 and Ida asteroids are presented for illustration. These results show that control of spacecraft along closed orbits, or to a fixed point is accomplished using each of these controllers, despite uncertainties in the parameters of the asteroid models.

*Professor, Department of Electronic Engineering, Catholic Kwandong University, Gangwon 25601, Republic of Korea. Email:kwlee@cku.ac.kr

†Professor, Department of Electrical and Computer Engineering, University of Nevada Las Vegas, Las Vegas, NV 89154-4026 (Corresponding Author). E-mail: sahjendra.singh@unlv.edu

Introduction

Scientific exploration of small bodies, such as asteroids and comets, is of considerable importance for understanding the origin and evolution of the solar system. In this respect, the National Aeronautics and Space Administration (NASA), the European Space Agency (ESA), and Japan Aerospace Exploration Agency have completed several asteroid missions, such as Galileo, Shoemaker, Cassini, Deepspace, Stardust, Hayabusa, and Rosetta, and are planning future missions to asteroids. NASA has special interest in transporting near-Earth asteroids to Halo orbits in the Earth-Moon system. For technological reasons, it is useful to identify and quantify asteroids as a source of extraterrestrial natural resources. In addition, transmitters stationed on asteroids can provide independent navigational capability for interplanetary flights.

Asteroids and comets have irregular shapes and a nonuniform mass distribution. The gravitational force of asteroid varies rapidly in intensity and direction as a function of the spatial coordinates of spacecraft orbiting around it. Mathematical modeling of an asteroid's gravitation force experienced by spacecraft has been of considerable interest. For the derivation of gravitational force, authors have developed models of gravitational potential in the form of an infinite series (Tricarico and Sykes 2010; Herrera-Sucarrat et al. 2013). The orbital dynamics of satellites around asteroids have been derived in several papers (Chauvineau et al. 1993; Scheeres 1994; Scheeres et al. 1996, 2000). The natural orbits around irregular rotating asteroids are not necessarily orbitally stable. Authors also have investigated the attitude dynamics of spacecraft orbiting around asteroids (Riverin and Misra 2002; Kumar 2008).

It is necessary to control the orbit and attitude of spacecraft around asteroids and comets to obtain accurate information about their surface characteristics, density, size, and spin rate. Researchers have designed closed-loop guidance laws for hovering motion and orbit control around celestial bodies (Sawai et al. 2002; Broschart and Scheeres 2005) by using linearized models. Based on MacCullagh's approximation of the gravitational potential field, Guelman (2015) obtained the equations of motion of a spacecraft around a small rotating celestial body, and designed a guidance law for orbit transfer and hovering in the equatorial plane. However, this control law is not capable of controlling the spacecraft to the unstable equilibrium point on the X_a-axis. In a recent paper, Guelman (2017) used spherical harmonics expansion of the gravitational potential field in the spacecraft dynamics, and obtained a control law for global control. A fuel optimal controller also has been designed for a soft landing on irregular asteroids (Yang and Baoyin 2015;

Hawkins et al. 2012). For optimal design, dynamics of the model are assumed to be known. Lee et al. (2015) designed a continuous finite-time control law for performing coupled translational and rotational maneuvers over a tumbling asteroid. Kumar (2008) proposed a linear state feedback control system for attitude control of a spacecraft orbiting around an asteroid. A multiple sliding surface nonlinear guidance algorithm, using higher-order sliding mode control theory, has been developed for powered descent and landing on asteroid (Furfaro et al. 2013). Based on a nonlinear terminal sliding surface, a guidance scheme has been proposed for hovering and landing in a finite time (Yang et al. 2017). These sliding modes control laws are not continuous. Also, it is necessary to avoid singularity by making approximations in the control law (Yang et al. 2017). It is well known that the discontinuity in the sliding mode control law causes an undesirable chattering phenomenon.

For the control of nonlinear systems with parameterized nonlinear functions, adaptive control schemes often are used (krstic et al. 1995). However, for robust control of nonlinear systems that include bounded unstructured uncertain functions, super-twisting (STW) sliding mode control laws are suitable (Levant 2005; Shtessel et al. 2014; Fridman et al. 2015, Moreno and Osorio 2012). The STW control signals are continuous functions of state variables. It appears from the published research that robust control systems, based on adaptive and STW algorithms, have not been designed for orbit control around asteroids having structured and unstructured uncertainties.

This paper focuses on the design of adaptive and robust control systems to enable the spacecraft to follow closed orbits around asteroids or to attain a fixed point. It is assumed that the irregularly shaped asteroid is rotating about an axis fixed to its body. Similar to Guelman (2015), the nonlinear dynamics of the spacecraft around the asteroid are based on the MacCullagh approximation of the gravitational potential field. This model includes first three terms of the infinite power series expansion (Schaub and Junkins 2003). Unlike Guelman (2015), however, the cross products of inertia are retained in the model for design. It is assumed that mass and the inertia matrix of the asteroid are not known.

The contributions of this paper are fourfold. First, an adaptive control law is designed to accomplish global asymptotic convergence of the relative position trajectory of the spacecraft to prescribed closed orbits around the asteroid. Second, a super-twisting adaptive (STWA) continuous control system for global asymptotic trajectory control is developed. This controller

includes a super-twisting control law for the nominal system and a parameter adaptation law to nullify the effect of uncertainties in the parameters. Third, under the assumption of boundedness of the derivative of the uncertain nonlinear functions in a region of the state space, an STW control system for finite-time convergence of the system trajectory to the closed orbit is presented. The stability properties of the closed-loop system, including each of these controllers, are analyzed using Lyapunov stability theory. Fourth, performance of these three control systems is examined for the control of spacecraft around Eros 433 and Ida asteroids. These results show that each of these control systems can achieve trajectory control despite uncertainties in the asteroid's model parameters.

Asteroid Dynamics and Control Problem

Figure 1 shows an irregularly shaped asteroid with a body-fixed axes (X_a, Y_a, Z_a), and an inertial coordinate system (X_I, Y_I, Z_I), with the origin at its center of mass. It is assumed that the asteroid is in pure rotation about axis Z_a. Let the relative position coordinates of a spacecraft in the (X_a, Y_a, Z_a) frame be (x, y, z).

The approximate gravitational potential of the asteroid, retaining only the first three terms of the infinite series expansion introduced by MacCullagh, is given by (Schaub and Junkins 2003)

$$V(r) = -\frac{Gm}{r} - \frac{G}{2r^3}[I_{11} + I_{22} + I_{33} - 3I_r]$$
$$I_r = \frac{1}{r^2}(x, y, z)\boldsymbol{I_a}(x, y, z)^T \tag{1}$$

where the superscript T denotes matrix transposition, $r = (x^2 + y^2 + z^2)^{1/2}$, G is the universal gravitational constant, m is the mass of the asteroid, and its inertia matrix is

$$\boldsymbol{I_a} = \begin{bmatrix} I_{11} & I_{12} & I_{13} \\ I_{12} & I_{22} & I_{23} \\ I_{13} & I_{23} & I_{33} \end{bmatrix}$$

The gravitational acceleration experienced by the spacecraft is given by

$$\boldsymbol{f_g} = -\nabla V = -\left(\frac{\partial V}{\partial x}, \frac{\partial V}{\partial y}, \frac{\partial V}{\partial z}\right)^T \tag{2}$$

Noting that $\nabla(1/r) = -(1/r^2)\hat{\boldsymbol{i}}_{\boldsymbol{r}}$, Eq. (2) gives

$$\boldsymbol{f_g} = -\frac{Gm}{r^2}\hat{\boldsymbol{i}}_{\boldsymbol{r}} - \frac{3G}{2r^4}\left[\sum_{i=1}^{3} I_{ii} - 5I_r\right]\hat{\boldsymbol{i}}_{\boldsymbol{r}} - \frac{3G}{r^5}\boldsymbol{I_a}(x, y, z)^T \tag{3}$$

where the unit directional vector expressed through the Cartesian vector components is $\hat{\boldsymbol{i}}_{\boldsymbol{r}} = r^{-1}(x, y, z)^T$. Expanding Eq. (3), and using some algebraic manipulation, one can show that

$$\boldsymbol{f_g} = -m\frac{G}{r^3}(x, y, z)^T - \frac{3G}{r^5}\boldsymbol{I_a}(x, y, z)^T$$

$$-\frac{3G}{2r^5}\begin{bmatrix} I_{11}x + I_{22}x + I_{33}x - \frac{5}{r^2}\{I_{11}x^3 + I_{22}y^2x + I_{33}z^2x + 2I_{12}x^2y + 2I_{13}x^2z + 2I_{23}xyz\} \\ I_{11}y + I_{22}y + I_{33}y - \frac{5}{r^2}\{I_{11}x^2y + I_{22}y^3 + I_{33}z^2y + 2I_{12}xy^2 + 2I_{13}xyz + 2I_{23}y^2z\} \\ I_{11}z + I_{22}z + I_{33}z - \frac{5}{r^2}\{I_{11}x^2z + I_{22}y^2z + I_{33}z^3 + 2I_{12}xyz + 2I_{13}xz^2 + 2I_{23}yz^2\} \end{bmatrix} \quad (4)$$

In view of Eq. (4), a linearly parameterized form of the gravitational acceleration takes the form

$$\boldsymbol{f_g} = \boldsymbol{\Phi}(x, y, z)\boldsymbol{\nu_a} \quad (5)$$

where the regressor matrix is $\boldsymbol{\Phi} = [\boldsymbol{\phi_1}, ..., \boldsymbol{\phi_7}] \in \boldsymbol{R}^{3\times7}$, the parameter vector is $\boldsymbol{\nu_a} = [m, I_{11}, I_{22}, I_{33}, I_{12}, I_{13}, I_{23}]^T \in \boldsymbol{R}^7$, and $\boldsymbol{\phi_i}(x, y, z) \in \boldsymbol{R}^3$, $(i = 1, ..., 7)$, are

$$\boldsymbol{\phi_1} = -\frac{G}{r^3}(x, y, z)^T$$

$$\boldsymbol{\phi_2} = -\frac{3G}{2r^5}\left(1 - \frac{5x^2}{r^2}\right)(x, y, z)^T - \frac{3G}{r^5}(x, 0, 0)^T$$

$$\boldsymbol{\phi_3} = -\frac{3G}{2r^5}\left(1 - \frac{5}{r^2}y^2\right)(x, y, z)^T - \frac{3G}{r^5}(0, y, 0)^T$$

$$\boldsymbol{\phi_4} = -\frac{3G}{2r^5}\left(1 - \frac{5z^2}{r^2}\right)(x, y, z)^T - \frac{3G}{r^5}(0, 0, z)^T$$

$$\boldsymbol{\phi_5} = \frac{15G}{r^7}xy(x, y, z)^T - \frac{3G}{r^5}(y, x, 0)^T$$

$$\boldsymbol{\phi_6} = \frac{15G}{r^7}xz(x, y, z)^T - \frac{3G}{r^5}(z, 0, x)^T$$

$$\boldsymbol{\phi_7} = \frac{15G}{r^7}yz(x, y, z)^T - \frac{3G}{r^5}(0, z, y)^T$$

Each element of the regressor matrix $\boldsymbol{\Phi}$ is a known function of the coordinates x, y, and z of the spacecraft in the body-fixed frame.

Define $\boldsymbol{x_{s1}} = (x, y, z)^T \in \boldsymbol{R}^3$ and $\boldsymbol{x_{s2}} = (\dot{x}, \dot{y}, \dot{z})^T$, and $\boldsymbol{x_s} = (\boldsymbol{x_{s1}}^T, \boldsymbol{x_{s2}}^T)^T \in \boldsymbol{R}^6$. Then the coordinates (x, y, z) of the spacecraft with respect to the asteroid, written in the body-fixed frame (X_a, Y_a, Z_a), can be shown to satisfy (Guelman 2015)

$$\dot{\boldsymbol{x}}_{\boldsymbol{s1}} = \boldsymbol{x_{s2}}$$

$$\dot{\boldsymbol{x}}_{\boldsymbol{s2}} = \begin{bmatrix} 2\omega\dot{y} + \omega^2 x \\ -2\omega\dot{x} + \omega^2 y \\ 0 \end{bmatrix} + \begin{bmatrix} -\frac{\partial V}{\partial x} \\ -\frac{\partial V}{\partial y} \\ -\frac{\partial V}{\partial z} \end{bmatrix} + \boldsymbol{a_c}$$
$$\doteq \boldsymbol{f_0}(x_s) + \boldsymbol{\Phi}(\boldsymbol{x_{s1}})\boldsymbol{\nu_a} + \boldsymbol{a_c} \tag{6}$$

where ω is the rotation rate of the asteroid, $\boldsymbol{a_c}(t) = (a_{c1}, a_{c2}, a_{c3})^T \in \boldsymbol{R}^3$ is the control input applied to the spacecraft, and the nonlinear vector function $\boldsymbol{f_0}(\boldsymbol{x_s})$ is given by

$$\boldsymbol{f_0} = (2\omega\dot{y} + \omega^2 x, -2\omega\dot{x} + \omega^2 y, 0)^T \in \boldsymbol{R}^3 \tag{7}$$

It is noted that Eq. (6) includes terms involving cross products of inertia as well; therefore, this model also is useful for the case in which X_a, Y_a, and Z_a are not the principal axes of inertia of the asteroid. It is assumed that the parameter vector $\boldsymbol{\nu_a}$ is not known. Here, the rotation rate ω is assumed to be a known constant for simplicity. However, such an assumption is not necessary, and ω could be included in $\boldsymbol{\nu_a}$ for design using a modified regressor matrix $\boldsymbol{\Phi}$.

Suppose that a smooth bounded reference trajectory $\boldsymbol{w_{1r}}(t) = (x_r, y_r, z_r)^T \in \boldsymbol{R}^3$ is given. It is desired to derive control laws so that the trajectory $(x, y, z)^T$ of the spacecraft converges to the reference trajectory $\boldsymbol{w_{1r}}(t)$, despite uncertainties in the parameter vector $\boldsymbol{\nu_a} \in \boldsymbol{R}^7$. The choice of the reference trajectory depends on the mission requirement. As an example, a spacecraft will hover over a fixed point of the asteroid if $\boldsymbol{w_{1r}}$ is a constant vector. For maintaining the spacecraft in a closed orbit around the asteroid, a periodic time-varying $\boldsymbol{w_{1r}}(t)$ is selected. In the sequel, the design of an adaptive, an STWA, and an STW control system is considered.

Adaptive Control Law

First, the design of an adaptive control system is considered. For the purpose of trajectory control, define the tracking error $\boldsymbol{w_1} = \boldsymbol{x_{s1}} - \boldsymbol{w_{1r}} = (w_{11}, w_{12}, w_{13})^T$, $\boldsymbol{w_2} = \dot{\boldsymbol{w}}_{\boldsymbol{1}} = (w_{21}, w_{22}, w_{23})^T$, and $\boldsymbol{w} = (\boldsymbol{w_1}^T, \boldsymbol{w_2}^T)^T \in \boldsymbol{R}^6$. Then, using Eq. (6), the tracking error dynamics can be written as

$$\dot{\boldsymbol{w}}_{\boldsymbol{1}} = \boldsymbol{w_2}$$
$$\dot{\boldsymbol{w}}_{\boldsymbol{2}} = \boldsymbol{f_0}(\boldsymbol{x_s}) + \boldsymbol{\Phi}(\boldsymbol{x_{s1}})\boldsymbol{\nu_a} + \boldsymbol{a_c} - \ddot{\boldsymbol{w}}_{\boldsymbol{1r}} \tag{8}$$

The uncertain parameter vector can be written as $\boldsymbol{\nu_a} = \boldsymbol{\nu^*} + \boldsymbol{\nu}$, where $\boldsymbol{\nu^*}$ is the nominal value and $\boldsymbol{\nu}$ is the uncertain part. Then in view of Eq. (8), one selects the control input $\boldsymbol{a_c}$ as

$$\boldsymbol{a_c} = -\boldsymbol{f_0}(\boldsymbol{x_s}) - \boldsymbol{\Phi}(\boldsymbol{x_{s1}})(\boldsymbol{\nu}^* + \hat{\boldsymbol{\nu}}) + \boldsymbol{u_s} + \ddot{\boldsymbol{w}}_{\boldsymbol{1r}} \tag{9}$$

where $\hat{\boldsymbol{\nu}}$ is an estimate of $\boldsymbol{\nu}$. The signal $\boldsymbol{u_s}$ in Eq. (9) is

$$\boldsymbol{u_s} = (u_{s1}, u_{s2}, u_{s3})^T = -k_1 \boldsymbol{w_1} - k_2 \boldsymbol{w_2} \tag{10}$$

where k_1 and k_2 are positive feedback gains. Define a matrix $\boldsymbol{B} = [\boldsymbol{0}_{3\times3}, \boldsymbol{I}_{3\times3}]^T$ and a Hurwitz matrix $\boldsymbol{A}$ as

$$\boldsymbol{A} = \begin{bmatrix} \boldsymbol{0}_{3\times3} & \boldsymbol{I}_{3\times3} \\ -k_1\boldsymbol{I}_{3\times3} & -k_2\boldsymbol{I}_{3\times3} \end{bmatrix} \tag{11}$$

Then, substituting the control law Eq. (9) in Eq. (8) gives

$$\dot{\boldsymbol{w}} = \boldsymbol{A}\boldsymbol{w} - \boldsymbol{B}\boldsymbol{\Phi}(\boldsymbol{x_{s1}})\tilde{\boldsymbol{\nu}} \tag{12}$$

where $\tilde{\boldsymbol{\nu}} = \hat{\boldsymbol{\nu}} - \boldsymbol{\nu} \in \boldsymbol{R}^7$ is the parameter error vector. At this point, the design of an adaptation law is considered.

Consider a positive definite quadratic Lyapunov function

$$W_s(\boldsymbol{w}, \tilde{\boldsymbol{\nu}}) = \boldsymbol{w}^T\boldsymbol{P}\boldsymbol{w} + \frac{1}{2}\tilde{\boldsymbol{\nu}}^T\boldsymbol{\Gamma}^{-1}\tilde{\boldsymbol{\nu}} \tag{13}$$

where $\boldsymbol{P}$ is a positive definite symmetric matrix (denoted as $\boldsymbol{P} > 0$) and $0 < \boldsymbol{\Gamma} \in \boldsymbol{R}^{7\times7}$ is the adaptation gain. Because the matrix $\boldsymbol{A}$ is Hurwitz, there exists a unique positive definite symmetric matrix $\boldsymbol{P}$, which is the solution of the Lyapunov equation

$$\boldsymbol{A}^T\boldsymbol{P} + \boldsymbol{P}\boldsymbol{A} = -\boldsymbol{Q} \tag{14}$$

for any given $\boldsymbol{Q} > 0$. Specifically for $\boldsymbol{Q} = \boldsymbol{I}_{6\times6}$, it can be verified that $\boldsymbol{P}$ given by

$$\boldsymbol{P} = \begin{bmatrix} p_1\boldsymbol{I}_{3\times3} & p_2\boldsymbol{I}_{3\times3} \\ p_2\boldsymbol{I}_{3\times3} & p_3\boldsymbol{I}_{3\times3} \end{bmatrix} \tag{15}$$

with

$$p_1 = \frac{k_1^2 + k_2^2 + k_1}{2k_1k_2}$$

$$p_2 = \frac{1}{2k_1}$$

$$p_3 = \frac{k_1 + 1}{2k_1k_2}$$

satisfies Eq. (14).

The derivative of W_s, along the solution of Eq. (12), takes the form

$$\dot{W}_s = \boldsymbol{w}^T[\boldsymbol{P}\boldsymbol{A} + \boldsymbol{A}^T\boldsymbol{P}]\boldsymbol{w} - 2\boldsymbol{w}^T\boldsymbol{P}\boldsymbol{B}\boldsymbol{\Phi}(\boldsymbol{x_{s1}})\tilde{\boldsymbol{\nu}} + \tilde{\boldsymbol{\nu}}^T\boldsymbol{\Gamma}^{-1}\dot{\tilde{\boldsymbol{\nu}}}$$

$$= -\boldsymbol{w}^T\boldsymbol{Q}\boldsymbol{w} + \tilde{\boldsymbol{\nu}}^T\boldsymbol{\Gamma}^{-1}(\dot{\tilde{\boldsymbol{\nu}}} - 2\boldsymbol{\Gamma}\boldsymbol{\Phi}^T(\boldsymbol{x_{s1}})\boldsymbol{P_2}^T\boldsymbol{w}) \tag{16}$$

where $\boldsymbol{P_2}^T = (p_2\boldsymbol{I}_{3\times3}, p_3\boldsymbol{I}_{3\times3})^T \in \boldsymbol{R}^{3\times6}$. In view of Eq. (16), an adaptation law is chosen as

$$\dot{\boldsymbol{\nu}} = \dot{\tilde{\boldsymbol{\nu}}} = 2\boldsymbol{\Gamma}\boldsymbol{\Phi}^T(\boldsymbol{x_{s1}})\boldsymbol{P_2}^T\boldsymbol{w} \tag{17}$$

Substituting the adaptation law Eq. (17) in Eq. (16) gives

$$\dot{W}_s = -\boldsymbol{w}^T\boldsymbol{Q}\boldsymbol{w} \leq 0 \tag{18}$$

The derivative of W_s is negative semidefinite. Therefore, all the signals in the closed-loop system are bounded. Then, using LaSalle-Yoshizawa theorem (Krstic et al. 1995), it can be shown that w asymptotically tends to zero for any initial condition.

Super-Twisting Adaptive Law

Now, the design of a super-twisting adaptive law is considered. The control system includes a super-twisting control module and a parameter adaptation law to counter the effect of uncertainties in the parameters. In contrast to the quadratic Lyapunov function given in Eq. (13), the STWA law is designed based on a nonlinear Lyapunov function (given in Fridman et al. 2015), which includes signals with fractional exponents.

Define a function s_i, $(i = 1, 2, 3)$, as

$$s_i = w_{2i} + k_2 sig(w_{1i})^{2/3} \tag{19}$$

where $k_2 > 0$; and for any scalar function v and an exponent μ, one defines $sig(v)^\mu = |v|^\mu sign(v)$. It can be easily verified that if $s_i = 0$, then w_{1i} will converge to zero in a finite time. The derivative of s_i is

$$\dot{s}_i = \dot{w}_{2i} + \frac{2}{3}k_2|w_{1i}|^{-1/3}w_{2i} \tag{20}$$

Now, based on the STW algorithm given in Fridman et al. (2015), the signal $\boldsymbol{u_s}$ is selected of the form

$$\boldsymbol{u_s} = -k_1 sig(\boldsymbol{s})^{1/2} + \boldsymbol{w_3} \tag{21}$$

where $\boldsymbol{w_3} = (w_{31}, w_{32}, w_{33})^T \in \boldsymbol{R}^3$ satisfies

$$\dot{\boldsymbol{w}}_{\boldsymbol{3}} = -k_3 sgn(\boldsymbol{s}) \tag{22}$$

and the feedback gains $k_1 > 0$, $k_3 > 0$, $\boldsymbol{s} = (s_1, s_2, s_3)^T$, $sign(\boldsymbol{s}) = (sign(s_1), sign(s_2), sign(s_3))^T$, and $sig(\boldsymbol{s})^\mu = (sig(s_1)^\mu, sig(s_2)^\mu, sig(s_3)^\mu)^T$. One notes that the signal $\boldsymbol{u_s}$ including the integral of $sign(\boldsymbol{s})$ is a continuous vector function. Using the control law Eqs. (9), (21) and (22) in Eq. (8) gives

$$\dot{\boldsymbol{w}}_{\boldsymbol{1}} = \boldsymbol{w_2}; \dot{\boldsymbol{w}}_{\boldsymbol{2}} = -k_1 sig(\boldsymbol{s})^{1/2} + \boldsymbol{w_3} - \boldsymbol{\Phi}\tilde{\boldsymbol{\nu}}$$

$$\dot{\boldsymbol{w}}_{\boldsymbol{3}} = -k_3 sgn(\boldsymbol{s}) \tag{23}$$

For analyzing the stability of the closed-loop system, new coordinates given by

$$\boldsymbol{\xi_i} = \begin{bmatrix} sig(w_{1i})^{2/3} \\ s_i \\ sig(w_{3i})^2 \end{bmatrix}, \boldsymbol{\xi_i} \in \boldsymbol{R}^3, (i = 1, 2, 3) \tag{24}$$

are introduced. Differentiating $\boldsymbol{\xi_i}$, and using $\dot{s}_i$ and $\dot{w}_{2i}$ from Eq. (20) and (23), gives

$$\dot{\xi}_i = \begin{bmatrix} \frac{2}{3}|w_{1i}|^{-1/3} w_{2i} \\ -k_1 sig(s_i)^{1/2} + w_{3i} + \frac{2}{3} k_2 |w_{1i}|^{-1/3} w_{2i} - \boldsymbol{\phi_{ri}}(\boldsymbol{x_{s1}})\tilde{\boldsymbol{\nu}} \\ -2k_3 |w_{3i}| sgn(s_i) \end{bmatrix} \tag{25}$$

where $\boldsymbol{\phi_{ri}}(\boldsymbol{x_{s1}})$ denotes the ith row of $\boldsymbol{\Phi}(\boldsymbol{x_{s1}})$.

Consider a quadratic function $W_i(\boldsymbol{\xi_i})$ for the $\boldsymbol{\xi_i}$-dynamics Eq. (25)

$$W_i(\boldsymbol{\xi_i}) = \boldsymbol{\xi_i}^T \boldsymbol{P_s} \boldsymbol{\xi_i} \tag{26}$$

where $\boldsymbol{P_s} \in \boldsymbol{R}^{3\times 3}$ is a symmetric matrix of the form

$$\boldsymbol{P_s} = \begin{bmatrix} p_1 & -\frac{1}{2}p_{12} & \frac{1}{2}p_{13} \\ -\frac{1}{2}p_{12} & p_2 & -\frac{1}{2}p_{23} \\ \frac{1}{2}p_{13} & -\frac{1}{2}p_{23} & p_3 \end{bmatrix} \tag{27}$$

The elements of the matrix $\boldsymbol{P_s}$ are selected such that $\boldsymbol{P_s}$ is a positive definite matrix. Differentiating W_i along the solution of Eq. (25) gives

$$\dot{W}_i = 2\boldsymbol{\xi_i}^T \boldsymbol{P_s} \begin{bmatrix} \frac{2}{3}|w_{1i}|^{-1/3} w_{2i} \\ -k_1 sig(s_i)^{1/2} + w_{3i} + \frac{2}{3} k_2 |w_{1i}|^{-1/3} w_{2i} \\ -2k_3 |w_{3i}| sgn(s_i) \end{bmatrix} + 2\boldsymbol{\xi_i}^T \boldsymbol{P_s} \begin{bmatrix} 0 \\ -\boldsymbol{\phi_{ri}}\tilde{\boldsymbol{\nu}} \\ 0 \end{bmatrix}$$

$$\doteq W_{id} - 2\boldsymbol{\xi_i}^T \boldsymbol{P_{s2}} \boldsymbol{\phi_{ri}} \tilde{\boldsymbol{\nu}} \tag{28}$$

where $\boldsymbol{P_{s2}}$ is the second column of matrix $\boldsymbol{P_s}$, and W_{id} is the value of $\dot{W}_i$ if $\tilde{\boldsymbol{\nu}}$ is zero. It has been shown by Fridman et al. (2015) that there exists a set of elements of the matrix $\boldsymbol{P_s}$, and the feedback gains $k_i > 0$, such that the following inequality holds:

$$W_{di} \leq -\kappa_i W_i^{3/4}(\boldsymbol{\xi_i}) \tag{29}$$

where $\kappa_i > 0$. This implies that the $\boldsymbol{\xi_i}$ system described by Eq. (25), without any parameter uncertainties (i. e., $\tilde{\boldsymbol{\nu}} = 0$), is finite-time stable (Bhat and Bernstein 2005); therefore, $\boldsymbol{\xi_i}$ tends to zero in a finite time. This finite-time convergence property of the system without uncertainties has been possible due the nonlinear stabilizing control signal $\boldsymbol{u_s}$. In contrast to this, the adaptive law (Eqs. (9), (10), and (17)) can accomplish only asymptotic convergence even for the uncertainty-free model.

Now, for the derivation of an adaptation law for the uncertain system, consider a composite Lyapunov function

$$W_a(\boldsymbol{\xi}, \tilde{\boldsymbol{\nu}}) = W(\boldsymbol{\xi}) + \frac{1}{2}\tilde{\boldsymbol{\nu}}^T \boldsymbol{\Gamma}^{-1} \tilde{\boldsymbol{\nu}}, \boldsymbol{\Gamma} > 0 \tag{30}$$

where $\boldsymbol{\xi} = (\xi_1^T, \xi_2^T, \xi_3^T)^T \in \boldsymbol{R}^9$, and

$$W(\boldsymbol{\xi}) = \sum_{i=1}^{3} W_i(\boldsymbol{\xi_i}) \tag{31}$$

$W(\boldsymbol{\xi})$ is a positive definite function of $\boldsymbol{\xi}$. Differentiating W_a and using Eq. (28) gives

$$\begin{aligned} \dot{W}_a &= \sum_{i=1}^{3} W_{id} - \left(\sum_{i=1}^{3} 2\boldsymbol{\xi_i}^T \boldsymbol{P_{s2}} \boldsymbol{\phi_{ri}} \right) \tilde{\boldsymbol{\nu}} + \tilde{\boldsymbol{\nu}}^T \boldsymbol{\Gamma}^{-1} \dot{\tilde{\boldsymbol{\nu}}} \\ &= \sum_{i=1}^{3} W_{id} + \tilde{\boldsymbol{\nu}}^T \boldsymbol{\Gamma}^{-1} \left[\dot{\tilde{\boldsymbol{\nu}}} - \boldsymbol{\Gamma} \left(\sum_{i=1}^{3} 2\boldsymbol{\phi}_{\boldsymbol{ri}}^T \boldsymbol{P}_{\boldsymbol{s2}}^T \boldsymbol{\xi_i} \right) \right] \end{aligned} \tag{32}$$

In view of Eq. (32), an adaptation law is selected as

$$\dot{\hat{\boldsymbol{\nu}}} = \dot{\tilde{\boldsymbol{\nu}}} = \boldsymbol{\Gamma} \sum_{i=1}^{3} 2\boldsymbol{\phi}_{\boldsymbol{ri}}^T \boldsymbol{P}_{\boldsymbol{s2}}^T \boldsymbol{\xi_i} \tag{33}$$

Substituting Eq. (33) in (32) and using Eq. (29) gives

$$\dot{W}_a = \sum_{i=1}^{3} W_{di} \leq -\sum_{i=1}^{3} \kappa_i W_i^{3/4}(\boldsymbol{\xi_i}) \leq 0 \tag{34}$$

The composite Lyapunov function $W_a(\boldsymbol{\xi}, \tilde{\boldsymbol{\nu}})$ is a positive definite function of $(\boldsymbol{\xi}, \tilde{\boldsymbol{\nu}})$ and $\dot{W}_a$ is negative semidefinite. Thus, all the signals in the closed-loop systems are bounded. One notices

that the derivative of W_a in Eq. (34) vanishes only if $\boldsymbol{\xi}$ is zero. Thus, it follows that in the closed-loop system, $\boldsymbol{\xi}$ asymptotically tends to zero. Now, based on the definition of $\boldsymbol{\xi}$ in Eq. (24), one concludes that $\boldsymbol{w_1}$, $\boldsymbol{s}$, and $\boldsymbol{w_3}$ also converge to zero asymptotically for any initial condition. Of course, convergence of $\boldsymbol{s}$ to zero implies that $\boldsymbol{w_2}$ tends to zero.

Super-Twisting Law

At this point, a super-twisting control law is obtained. This control law does not use parameter adaptation. An assumption is made for the design of this control law.

Assumption 1: It is assumed that the trajectory of the system evolves in an arbitrarily large region $\boldsymbol{\Omega_s} \subset \boldsymbol{R}^6$, in which

$$\left| \frac{d\boldsymbol{\phi_{rj}}(\boldsymbol{x_{s1}})\boldsymbol{\nu}}{dt} \right| < \rho < \infty, j = 1, 2, 3 \tag{35}$$

for some $\rho > 0$.

Here, the design of the STW law is briefly presented for completeness. (Readers may refer to Fridman et al. (2015) for the details of derivation.) The STW control law is selected as

$$\boldsymbol{a_c} = -\boldsymbol{f_0}(\boldsymbol{x_s}) - \boldsymbol{\Phi}(\boldsymbol{x_{s1}})\boldsymbol{\nu^*} + \boldsymbol{u_s} + \ddot{\boldsymbol{w}}_{\boldsymbol{1r}}$$

$$\boldsymbol{u_s} = -k_1 sig(\boldsymbol{s})^{1/2} + \boldsymbol{w_3}$$

$$\dot{\boldsymbol{w}}_{\boldsymbol{3}} = -k_3 sgn(\boldsymbol{s}) \tag{36}$$

It can be noted that this STW control signal does not use $\hat{\boldsymbol{\nu}}$, unlike the STWA control law. Then, the closed-loop system takes the form

$$\dot{\boldsymbol{w}}_{\boldsymbol{1}} = \boldsymbol{w_2}; \dot{\boldsymbol{w}}_{\boldsymbol{2}} = -k_1 sig(\boldsymbol{s})^{1/2} + \boldsymbol{w_3} + \boldsymbol{\Phi}(\boldsymbol{x_{s1}})\boldsymbol{\nu}$$

$$\dot{\boldsymbol{w}}_{\boldsymbol{3}} = -k_3 sgn(\boldsymbol{s}) \tag{37}$$

It is seen that the discontinuous signal $k_3 sign(\boldsymbol{s})$ appears in $\dot{\boldsymbol{w}}_{\boldsymbol{3}}$. For the stability analysis, a new variable defined as

$$\boldsymbol{w_{3m}} = \boldsymbol{w_3} + \boldsymbol{\Phi}(\boldsymbol{x_{s1}})\boldsymbol{\nu} \in \boldsymbol{R}^3 \tag{38}$$

is introduced. Then, the system Eq. (37) can be represented as

$$\dot{\boldsymbol{w}}_{\boldsymbol{1}} = \boldsymbol{w_2}; \dot{\boldsymbol{w}}_{\boldsymbol{2}} = -k_1 sig(\boldsymbol{s})^{1/2} + \boldsymbol{w_{3m}}$$

$$\dot{\boldsymbol{w}}_{\boldsymbol{3m}} = -k_3 sgn(\boldsymbol{s}) + \frac{d\boldsymbol{\Phi}(\boldsymbol{x}_{\boldsymbol{s1}})}{dt}\boldsymbol{\nu} \tag{39}$$

For the stability analysis, one similarly defines a new vector

$$\boldsymbol{\xi_{im}} = \begin{bmatrix} sig(w_{1i})^{2/3} \\ s_i \\ sig(w_{3mi})^2 \end{bmatrix}, \boldsymbol{\xi_{im}} \in \boldsymbol{R}^3, i = 1, 2, 3 \tag{40}$$

where w_{3mi} is the ith element of $\boldsymbol{w_{3m}}$. Then, under Assumption 1, it can be shown that there exist $\boldsymbol{P_s} > 0$, gains k_i, and Lyapunov functions $W_i = \boldsymbol{\xi_{im}^T P_s \xi_{im}}$, $(i = 1, 2, 3)$, such that

$$\dot{W}_i \leq -\kappa_m W_i^{3/4}, i = 1, 2, 3 \tag{41}$$

for some $\kappa_m > 0$. Solving the differential inequality Eq. (41), one finds that W_i converges to zero in a finite time T_{if} given by

$$T_{if} \leq \frac{4}{\kappa_m} W_i^{1/4}(\boldsymbol{\xi_{im}}(0)), i = 1, 2, 3$$

Therefore, according to Eqs. (19) and (40) , it is easily seen that $\boldsymbol{w_1}$ and $\boldsymbol{w_2}$ converge to zero in a finite time T_f, where $T_f = max\{T_{1f}, T_{2f}, T_{3f}\}$.

To this end, a discussion on the structure of each control law (adaptive, STWA, and STW) is provided. The control input $\boldsymbol{a_c}$ for adaptive control in Eq. (9) includes nominal (known) signals, adaptive $\hat{\boldsymbol{\nu}}$-dependent signal, and a stabilizing signal $\boldsymbol{u_s}$ (Eq. (10)). The signal $\boldsymbol{u_s}$ introduces proportional and derivative feedback of the error $\boldsymbol{w_1}$. The control acceleration $\boldsymbol{a}_c$ for STWA control is similar to Eq. (9), but its component $\boldsymbol{u_s}$ given in Eq. (21) is based on the super-twisting algorithm. Also, $\boldsymbol{u}_s$ includes a function $\boldsymbol{w}_3$ which is integral of a switching function $(-k_3 sign(\boldsymbol{s}))$ (see Eq. (22)). Furthermore its parameter adaptation law (Eq. (33)) differs from the parameter update law (Eq. (17)) of the adaptive system. The control acceleration $\boldsymbol{a_c}$ of the STW law consists of nominal signals and the signal $\boldsymbol{u_s}$ (see Eq. (36)). The signal $\boldsymbol{u_s}$ of the STW law is also based on the super-twisting control algorithm, but its gains (k_1, k_3) are not necessarily equal to the gains used for the STWA control. Unlike the adaptive and STWA systems, the STW control system does not use any parameter adaptation scheme.

Remark 1: The adaptive law and the STWA law accomplish global asymptotic convergence of the trajectory error to zero. The STW law has been derived for finite-time convergence of the tracking error under the assumption that the trajectories of the system evolve in an arbitrarily

large region $\boldsymbol{\Omega_s} \subset \boldsymbol{R}^6$, in which the uncertain functions satisfy $|(d\boldsymbol{\phi_{ri}}/dt)\boldsymbol{\nu}| \leq \rho$, $i = 1, 2, 3$. It can be pointed out that the uncertainty bounding parameter ρ increases with the size of $\boldsymbol{\Omega_s}$, and therefore, larger gains (k_1, k_2, k_3) are needed to preserve stability in the system (Fridman et al. 2015). In contrast to this, the feedback gains of the adaptive and STWA laws are independent of the values of the uncertain parameter vector $\boldsymbol{\nu}$.

Simulation Results

In this section, control of a spacecraft around asteroids using the adaptive, STWA, and STW control systems is considered. For the purpose of illustration, the models of Eros 433 and Ida of Wie (2015) and Guelman (2015), respectively, are used for simulation. (The parameters of these two asteroids are shown in Table 1 and Table 2.) The model of Eros 433 includes nonzero cross products of inertia, but the inertia matrix of Ida is diagonal. The objective is to track a closed orbit (not necessarily in the equatorial plane) described by a reference trajectory $\boldsymbol{w_{1r}}(t) = (x_r(t), y_r(t), z_r(t))^T$. As a representative example, a reference trajectory given by

$$x_r = 0.5R_d \sin(\omega_e t), y_r = R_d \cos(\omega_e t), z_r = R_d \sin(\omega_e t) \tag{42}$$

where the chosen values are $R_d = 35$ [km] and $\omega_e = 1.974\omega$ [rad/s]. (ω is the rotation rate of the asteroid.) For shaping transient responses, a modified trajectory $\boldsymbol{w_{1c}} = (x_c(t), y_c(t), z_c(t))^T$ given by

$$\boldsymbol{w_{1c}}(t) = \boldsymbol{x_{s1}}(0)e^{-\alpha_1 t^3} + \boldsymbol{w_{1r}}(t)(1 - e^{-\alpha_2 t^3}) \tag{43}$$

is generated. Because $\boldsymbol{w_{1c}}$ converges to $\boldsymbol{w_{1r}}$, it suffices to track $\boldsymbol{w_{1c}}$ to achieve orbit control. The choice of the parameters (α_1, α_2) affects the response characteristics. The chosen values are $\alpha_1 = \alpha_2 = 10^{-8}$. In the sequel, simulation results are obtained by using command shaping as well as without command shaping.

The nominal value of the parameter vector $\boldsymbol{\nu_a}$ is assumed to be $\boldsymbol{\nu}^* = 0.5\boldsymbol{\nu_a}$. The estimated initial value of $\boldsymbol{\nu}$ is set as $\hat{\boldsymbol{\nu}}(0) = 0$. Thus, 50% uncertainty in the parameter vector is assumed. The feedback gains of the adaptive law are $k_1 = w_s^2, k_2 = 2\zeta w_s, w_s = 0.1$, and $\zeta = 0.707$. For the adaptive law, the elements of the matrix $\boldsymbol{P}$ in Eq. (15) are $p_1 = 10.642, p_2 = 50$, and $p_3 = 357.0889$. For the STWA and STW control systems, the elements of matrix $\boldsymbol{P_s}$ in Eq. (27) given in Friedman et al. (2015) are used. These are $p_1 = 20, p_2 = 0.5, p_3 = 0.01, p_{12} = 1, p_{13} = 0.05$, and $p_{23} = 0.05$. The design parameters of the STWA and STW laws

are $k_1 = 0.06, k_2 = 0.01, k_3 = 0.01$. For digital implementation of the STWA and STW laws, the function $sgn(s_i)$ in Eqs. (22) and (36) is approximated by a saturation function $sat(s_i)$, where $sat(s_i) = (s_i/\epsilon)$, if $|s_i| \leq \epsilon$; and $sat(s_i) = sign(s_i)$, if $|s_i| > \epsilon$. The value of ϵ is 0.05. Of course, there exists a set of feedback and adaptation gains that can satisfy sufficient conditions for stability. However, for any practical system, it is essential to tune these gains to obtain acceptable responses. Here, as usual, the selection of the controller parameters has been made based on the observation of simulated responses.

***Case A*. Adaptive, STWA, and STW control of orbit around Eros 433**

The objective is to steer the spacecraft to the target orbit, specified by Eq. (42), around Eros 433. For this purpose, trajectory control along the modified trajectory $\boldsymbol{w_{1c}}$, which is obtained by command shaping using Eq. (43), is considered. First, the closed-loop system, which includes the spacecraft dynamics Eq. (6) and the adaptive law (Eqs. (9), (10), and (17)), is simulated. The initial conditions of the spacecraft are $\boldsymbol{x_{s1}}(0) = [2, 32, 4]^T$ [km] and $\boldsymbol{x_{s2}}(0) = [-0.00136, 0.000105, 0.00114]^T$ [km/s]. The initial value of the parameter estimate is $\hat{\boldsymbol{\nu}}(0) = \mathbf{0}_{7\times1}$, and the adaptation gain is $\boldsymbol{\Gamma} = diag(1, 2, 1, 2, 1, 2, 1)$.

The responses of the closed-loop adaptive system are shown in Figs. 2 and 3. (Unlike all other figures, the coordinates $x(t)$, $y(t)$, and $z(t)$ of the spacecraft are plotted over a longer period to show their waveforms while the spacecraft makes full rotations around the asteroid.) The 3-D plot in Fig. 3 shows that the trajectory (x, y, z) converges to the closed orbit. Fig. 2 (a) shows periodic waveforms of the spatial coordinates (x, y, z) in the steady state. The maximum value of the tracking error $(x-x_r, y-y_r, z-z_r)$ in steady state (denoted as $\boldsymbol{e_{ss}}$) is $[-0.0396, 0.0113, -0.0791]^T$ [km]. The maximum value (denoted as $\boldsymbol{a_{cm}}$) of control input over the whole interval and its peak value (denoted as $\boldsymbol{a_{cs}}$) in the steady state are $[0.1919, -0.0208, -0.1614]^T \times 10^{-3}$ [km/s^2] and $[-0.1518, -0.3497, -0.4376]^T \times 10^{-4}$ [km/s^2], respectively. It is seen in Fig. 2 that the tracking error remains close to zero beyond 800 seconds. For this selected maneuver, the $\Delta V(800)$ is 0.0916 [km/s], where $\Delta V(t) = \int_0^t \sum_1^3 |a_{ci}(\tau)| d\tau$. Of course, a small nonzero control input $\boldsymbol{a_c}(t)$ is required to keep the spacecraft moving along the closed orbit because $\boldsymbol{w_{1r}}(t)$ is not a natural trajectory of the system Eq. (6) with $\boldsymbol{a_c} = 0$. In fact, the $\Delta V(T_p)$ to maintain the spacecraft on the closed orbit for one period T_p ($T_p = 2\pi/\omega_e = 9.6109 \times 10^3[s]$) is 0.4841 [km/s]. The norm $||\hat{\nu}||$ of the estimated parameter vector remains bounded.

Now, for Eros 433, the STWA control law (Eqs. (9), (21), (22), (33)) is implemented.

Selected responses are shown in Fig. 4. The periodic waveform of (x, y, z) coordinates is observed. A smoothly converging waveform of the tracking error is observed. The tracking error is close to zero in about 800 [sec], and the required $\Delta V(800)$ is 0.4388 [km/s]. The values for $\boldsymbol{e_{ss}}$, $\boldsymbol{a_{cm}}$, and $\boldsymbol{a_{cs}}$ are $[-0.0402, 0.0100, -0.0804]^T$ [km], [0.0022, -0.0006, -0.0020]^T [km/s^2], and $[0.5752, 0.5671, 0.5969]^T \times 10^{-3}$ [km/s^2], respectively.

For Eros 433, simulated responses using the STW control law (Eq. (36)) are shown in Fig. 5. It is seen that the trajectory converges to the reference orbit. The peak value $\boldsymbol{e_{ss}}$ of the tracking error in the steady state is $[-0.0403, 0.0100, -0.0806]^T$ [km]. Fig. 5 shows that the tracking error is close to zero at 800 seconds. The required $\Delta V(800)$ is 0.4388 [km/s]. The control magnitudes are $\boldsymbol{a_{cm}} = [0.0022, -0.0006, -0.0020]^T$ [km/s^2] and $\boldsymbol{a_{cs}} = [-0.5774, -0.5988, -0.6067]^T \times 10^{-3}$ [km/s^2]. The performance characteristics of the adaptive, STWA, and STW laws observed in Figs. 2-5 for orbit control around Eros 433 are summarized in Table 3.

The closed-loop responses in Figs. 2 - 5 have been obtained by using command shaping. Now, direct control of the spacecraft along the reference trajectory (x_r, y_r, z_r) (without command shaping) is considered. The responses obtained using the STWA law for Eros 433 are shown in Fig. 6. One observes that the spacecraft follows the reference orbit. The tracking error converges close to zero in about 400 [s]. The $\Delta V(400)$ is 0.2579/[km/s]. The value of $||\boldsymbol{a_{cm}}||$ is 0.0102 [km/s^2]. Also, simulation has been done using the adaptive and STW laws without command shaping for control around Eros 433. These responses are not shown here in order to save space; however, the performance characteristics are provided in Table 4.

***Case B.* Adaptive, STWA, and STW control of orbit around Ida**

Now, orbit control around Ida asteroid using command shaping is considered. The model parameters given in Guelman (2015) are used for computation (see Table 2). For control around Ida, the initial estimate of the parameter vector is $\hat{\boldsymbol{\nu}}(0) = 0_{4\times1}$, and the adaptation gain is $\boldsymbol{\Gamma} = diag(1, 2, 1, 2)$. The controller feedback gains, initial conditions, and reference trajectory used for Eros 433 are retained. The selected responses obtained using adaptive law are shown in Fig. 7. The response characteristics are somewhat similar to those seen for Eros 433. The maximum values are $\boldsymbol{e_{ss}} = [-0.0453, 0.0225, -0.0903]^T$ [km], $\boldsymbol{a_{cm}} = [-0.2085, -0.5272, -0.4469]^T \times 10^{-3}$ [km/s^2], and $\boldsymbol{a_{cs}} = [-0.2085, -0.5272, -0.4469]^T \times 10^{-3}$ [km/s^2]. The tracking error is close to zero in about 800 [s]. The $\Delta V(800)$ is 0.4188[km/s]. One observes a periodic waveform of $\boldsymbol{a_c}$ in the terminal phase. This time-varying control acceleration is essential to maintain the spacecraft

on the closed orbit under the influence of varying gravitation force of Ida on the spacecraft. In fact, the $\Delta V(T_p)$ required to maintain the spacecraft on the closed orbit over one period is 5.6621 [km/s]. Of course, ΔV depends on the trajectory $\boldsymbol{w_{1r}}(t)$.

The responses obtained using the STWA law are shown in Fig. 8. The maximum values are $\boldsymbol{e_{ss}} = [-0.0467, 0.0181, -0.0934]^T$ [km], $\boldsymbol{a_{cm}}$=[0.0022, -0.0007 , -0.0020]^T [km/s^2], and $\boldsymbol{a_{cs}} = [-0.4088, 0.7098, -0.6274]^T \times 10^{-3}$ [km/s^2]. The input $\boldsymbol{a_c}$ is oscillating within 7×10^{-4}[km/s^2] and the $\Delta V(800)$ is 0.4210 [km/s].

The results of simulation of the closed-loop system, including the STW law, are shown in Fig. 9. The maximum values are $\boldsymbol{e_{ss}}$=[-0.0467, 0.0181, -0.0934]^T [km], $\boldsymbol{a_{cm}}$=[0.0022, -0.0007, -0.0020]^T [km/s^2], and $\boldsymbol{a_{cs}}$=[0.0013, 0.0016, -0.0009]^T [km/s^2]. The input $\boldsymbol{a_c}$ is oscillating within 1×10^{-3}[km/s^2] and $\Delta V(800)$ is 0.9583 [km/s]. The performance characteristics of the adaptive, STWA, and STW laws observed in Figs. 7-9 for orbit control around Ida by using command shaping are summarized in Table 5.

Simulation also has been done for direct orbit control around Ida without command shaping. The performance characteristics observed in the simulated responses are summarized in Table 6. Also, simulation has been performed for control around Ida using larger and smaller gains (k_1, k_2, k_3). Table 7 and Table 8 summarize the results.

Case C. **Spacecraft regulation to a fixed point for Ida**

Finally, simulation is done to regulate the spacecraft to an equilibrium point $\boldsymbol{w_{1r}} = (x_e, 0, 0)^T$ [km], located along the axis of minimum moment of inertia of Ida asteroid, using the adaptive control law (with command shaping). Guelman (2015) has shown that the equilibrium value x_e located outside the asteroid is the largest positive solution of

$$\omega^2 x_e^5 - Gmx_e^2 - \frac{3}{2}G(I_{22} + I_{33} - 2I_{11}) = 0 \tag{44}$$

The value of x_e for Ida is 32.2380 [km]. The initial conditions for $\boldsymbol{x_{s1}}$ and $\boldsymbol{x_{s2}}$, and the adaptive law of Case A are retained. Simulated responses in Fig. 10 show that the trajectory converges to the equilibrium point despite large initial tracking error. The required $\Delta V(800)$ is 0.3560 [km/s]. Also, simulated responses show that the spacecraft can be regulated to the equilibrium point by using the STWA and STW laws. The values of $\Delta V(800)$ for the STWA and STW laws are 0.4167 [km/s] and 0.9247 [km/s], respectively. c

To this end, a comparison of the performance of the adaptive, STWA, and STW control systems is provided. Observing the responses in Figs. 2-10 and the Tables 3-8, it is found that

each of the controllers is capable of achieving orbit control. Unlike the STWA and STW laws, the control acceleration $\boldsymbol{a_c}$ varies smoothly in the adaptive system. Although the STWA and STW laws attenuate control chattering, they are not able to suppress it completely. However, compared to the STWA law, the STW law shows stronger chattering effect. Based on the values of $(||\boldsymbol{a_{cm}}||, ||\boldsymbol{a_{cs}}||, \Delta V(800))$ in Table 3 and Table 5 (with command shaping), it is found that the adaptive law performs better than the STWA and STW laws. But the results of Table 4 and Table 6, and the responses of Fig. 6, obtained without command shaping, show that the STWA law gives better performance than the adaptive and STW laws. It is also seen that convergence time is shorter and ΔV is smaller, if command shaping is not used (see Table 4, Table 6, and Fig. 6); but the peak magnitude $||\boldsymbol{a_{cm}}||$ of the control input is slightly larger. It is interesting to observe that the ΔV required for maneuver using the STWA law is either smaller or equal to those required by the STW law (see Tables 3-6). Also, it may be noted that STW signals in the STWA and STW laws can provide robustness in the presence of external disturbance inputs. The value of ΔV depends on the initial state of the spacecraft, the target orbit, and the design parameters of the control laws. Of course, there exists flexibility in the choice of the design parameters to obtain trade-off among the response characteristics. Table 7 and Table 8 (with command shaping) show that smaller gains of the STWA and STW laws are useful in reducing the peak value of $||\boldsymbol{a_c}||$. It can be pointed out that from the viewpoint of simplicity in implementation, the STW law is preferable than the adaptive and STWA laws. However, simultaneous use of STW signal and parameter adaptation in the STWA system can provide flexibility in obtaining satisfactory performance.

Conclusions

In this paper, an adaptive law, an STWA law, and an STW law were developed for control of spacecraft around irregularly shaped asteroids. The mass and inertia matrix of the asteroid were assumed to be unknown. In the closed-loop system, the adaptive and STWA control laws accomplished global asymptotic trajectory control. Although the STW law achieved finite-time control for the system evolving in any arbitrary large region of the state space, the stabilizing gains of the control system vary with the size of the region. The Lyapunov approach was used for stability analysis for each closed-loop system. Simulation results showed that each control law can accomplish orbit control. Although there exists flexibility in the choice of design parameters

in each control law for shaping responses, the STWA law has advantage because it includes not only the STW signal but also an adaptive feedback signal.

Table 1. Mass, moments of inertia, and rotation rate of Eros 433 asteroid

Characteristics	Value	Characteristics	Value
Body mass m	6.6871×10^{15} [kg]	I_{11}	1.117×10^{17} [kg·km^2]
I_{22}	4.793×10^{17} [kg·km^2]	I_{33}	4.987×10^{17} [kg·km^2]
I_{12}	6.232×10^{16} [kg·km^2]	I_{13}	-2.257×10^{14} [kg·km^2]
I_{23}	-2.589×10^{13} [kg·km^2]	Rotational rate ω	3.312×10^{-4} [rad/s]

Table 2. Mass, moments of inertia, and rotation rate of Ida asteroid

Characteristics	Value	Characteristics	Value
Body mass m	5.1732×10^{16} [kg]	I_{11}	2.6306×10^{18} [kg·km^2]
I_{22}	9.2523×10^{18} [kg·km^2]	I_{33}	9.6015×10^{18} [kg·km^2]
I_{12}	0	I_{13}	0
I_{23}	0	Rotational rate ω	3.77×10^{-4} [rad/s]

Table 3. Performance of the adaptive, STWA, and STW control laws: peak values of tracking error and control input ($||\boldsymbol{e_{ss}}||, ||\boldsymbol{a_{cm}}||, ||\boldsymbol{a_{cs}}||$), ΔV for Eros 433 asteroid (with command shaping)

Control law	$||\boldsymbol{e_{ss}}||$[km]	$||\boldsymbol{a_{cm}}||$[km/s^2]	$||\boldsymbol{a_{cs}}||$[km/s^2]	$\Delta V(800)$ [km/s]
Adaptive	0.0892	2.5166×10^{-4}	5.8035×10^{-5}	0.0916
STWA	0.0905	0.0031	0.0010	0.4388
STW	0.0906	0.0031	0.0010	0.4388

Table 4. Performance of the adaptive, STWA, and STW control laws: peak values of tracking error and control input ($||\boldsymbol{e_{ss}}||, ||\boldsymbol{a_{cm}}||, ||\boldsymbol{a_{cs}}||$), and ΔV for Eros 433 asteroid (without command shaping)

Control law	$\|\|\boldsymbol{e_{ss}}\|\|$[km]	$\|\|\boldsymbol{a_{cm}}\|\|$[km/s^2]	$\|\|\boldsymbol{a_{cs}}\|\|$[km/s^2]	$\Delta V(400)$ [km/s]
Adaptive	0.0018	0.0509	4.8003×10^{-5}	0.8295
STWA	0.0164	0.0102	0.0010	0.2579
STW	0.0165	0.0102	0.0010	0.2579

Table 5. Performance of the adaptive, STWA, and STW control laws: peak values of tracking error and control input ($||\boldsymbol{e_{ss}}||, ||\boldsymbol{a_{cm}}||, ||\boldsymbol{a_{cs}}||$), and ΔV for Ida asteroid (with command shaping)

Control law	$\|\|\boldsymbol{e_{ss}}\|\|$[km]	$\|\|\boldsymbol{a_{cm}}\|\|$[km/s^2]	$\|\|\boldsymbol{a_{cs}}\|\|$[km/s^2]	$\Delta V(800)$ [km/s]
Adaptive	0.1035	7.2192×10^{-4}	7.2192×10^{-4}	0.4188
STWA	0.0160	0.0031	0.0010	0.4210
STW	0.1059	0.0031	0.0022	0.9583

Table 6. Performance of the adaptive, STWA, and STW control laws: peak values of tracking error and control input ($||\boldsymbol{e_{ss}}||, ||\boldsymbol{a_{cm}}||, ||\boldsymbol{a_{cs}}||$), and ΔV for Ida asteroid (without command shaping)

Control law	$\|\|\boldsymbol{e_{ss}}\|\|$[km]	$\|\|\boldsymbol{a_{cm}}\|\|$[km/s^2]	$\|\|\boldsymbol{a_{cs}}\|\|$[km/s^2]	$\Delta V(400)$ [km/s]
Adaptive	0.0352	0.0505	7.1826×10^{-4}	0.8753
STWA	0.0166	0.0096	0.0011	0.1786
STW	0.0166	0.0096	0.0020	0.4909

Table 7. Performance of the STWA and STW control laws with command shaping: peak values of tracking error and control input ($||\boldsymbol{e_{ss}}||, ||\boldsymbol{a_{cm}}||, ||\boldsymbol{a_{cs}}||$) for Ida with larger gains k_2 and k_3 ($k_1 = 0.06, k_2 = 0.1; k_3 = 0.1$)

Control law	$\|\|\boldsymbol{e_{ss}}\|\|$[km]	$\|\|\boldsymbol{a_{cm}}\|\|$[km/s^2]	$\|\|\boldsymbol{a_{cs}}\|\|$[km/s^2]	$\Delta V(800)$ [km/s]
STWA	0.1060	0.0036	0.0011	0.4905
STW	0.1060	0.0034	0.0025	0.9427

Table 8. Performance of the STWA and STW control laws with command shaping: peak values of tracking error and control input ($||\boldsymbol{e_{ss}}||, ||\boldsymbol{a_{cm}}||, ||\boldsymbol{a_{cs}}||$) for Ida with smaller gains ($k_1 = 0.01, k_2 = 0.001; k_3 = 0.001$)

Control law	$\|\|\boldsymbol{e_{ss}}\|\|$[km]	$\|\|\boldsymbol{a_{cm}}\|\|$[km/s^2]	$\|\|\boldsymbol{a_{cs}}\|\|$[km/s^2]	$\Delta V(800)$ [km/s]
STWA	0.1040	7.2338×10^{-4}	7.2338×10^{-4}	0.3733
STW	0.1040	7.3789×10^{-4}	7.3789×10^{-4}	0.3733

References

Bhat, S. P., and Bernstein, D. S. (2005). "Geometric homogeneity with applications to finite-time stability." *Math. Contr. Signals Systems*, 17, 101-127.

Broschart, S. B., and Scheeres, D. J. (2005). " Control of hovering spacecraft near small bodies: application to asteroid 25143 Itokawa." *J. of Guidance Control Dyn.* 25(4), 786-795.

Chauvineau, B., Farinella, P., and Mignard, F. (1993)."Planar orbits about a triaxial body: application to asteroidal satellites" *Icarus.* 105(2), 370-384.

Fridman, L., Moreno, J. A., Bandyopadhyay, B., Kamal, S., and Chalanga, A. (2015). "Continuous nested algorithms: the fifth generation of sliding mode controllers." *Recent Advances in Sliding Modes.* Springer, Switerland.

Furfaro, R., Cersosimo, D., and Wibben. (2013). "Asteroid precision landing via multiple sliding surfaces guidance techniques." *J. of Guidance Control Dyn.* 36(4), 1075-1092.

Guelman, M. (2015). "Closed-loop control of close orbits around asteroids." *J. Guidance Control Dyn.* 38(5), 854-860.

Guelman, M. (2017). "Closed-loop control for global coverage and equatorial hovering about an asteroid." *Acta Astronautica* 137, 353-361.

Herrera-Sucarrat, E., Palmer, P. L., and Roberts, R. M. (2013). "Modeling the gravitational potential of a nonspherical asteroid" *J. Guidance Control Dyn.* 36(3), 790-798.

Hawkins, M., Guo, Y., and Wie, B. (2012). "ZEM/ZEV feedback guidance application to fuel-optimal orbital maneuvers around an irregular-shaped asteroid." *Proc. AIAA Guidance Navigation Control Conf. and Exhibit* American Institute of Aeronautics and Astronautics , Reston, VA., 1-24.

Krstic, M., Kanellakopoulos., and Kokotovic, P. (1995). *Nonlinear and adaptive control design.* John Wiely, New York.

Kumar, K. D. (2008). "Attitude dynamics and control of satellites orbiting rotating asteroids," *Acta Mechanica.* 198(12), 99-118.

Lee, D., Sanyal, A. K., Butcher, E. A., and Scheeres, D. J. (2015). "Finite-time control for spacecraft body-fixed hovering over an asteroid." *IEEE Trans. Aerosp. Electronic.* 51(1), 506-518.

Levant, A. (2005). " Homogeneity approaches to higher-order sliding mode design." *Automatica.* 41, 823-830.

Moreno, J. A., and Osorio, M. (2012). "Strict Lyapunov functions for the super-twisting algo-

rithm." *IEEE Trans. Aut. Control.* 57(4), 1035-1040.

Riverin, J. L., and Misra, A. K. (2002). " Attitude dynamics of satellites orbiting small bodies." *AIAA/AAS Astrodyn. Specialist Conf. Exhibit.* AIAA 2002-4520.

Schub, H., and Junkins, J. L. (2003). *Analytical mechanics of space systems.* American Institute of Aeronautics and Astronautics, VA.

Sawai, S.,, Scheeres, D. J., and Broschart.(2002). " Control of hovering spacecraft using altimetry." *J. of Guidance Control Dyn.* 25(4), 786-795.

Scheeres, D. J. (1994)."Dynamics about uniformly rotating triaxial ellipsoids: applications to asteroids." *Icarus* 110(2), 225238.

Scheeres, D. J., Ostro, S. J., Hudson, R. S., and Werner, R. A. (1996). "Orbits close to asteroid 4769 Castalia." *Icarus.* 1211, 6787.

Scheeres, D. J., Williams, B. G., and Miller, J. K. (2000). "Evaluation of the dynamic environment of an asteroid: applications to 433 Eros." *J. of Guidance Control Dyn.* 23(3), 466-475.

Shtessel, Y., Edwards, C., Fridman, L., and Levant, A. (2014). *Sliding mode control and observation.* Springer, NY.

Tricarico, P., and Sykes, M. V. (2010)."Dynamical environment of Dawn at Vesta." *Planetary Space Science.* 58(12), 15161525.

Yang, H. and Baoyin. (2015). "Fuel-optimal control of soft landing on an irregular asteroid." *IEEE Trans. Aerosp. Electr. Systems.* 2015(3), 1688-1697.

Wie, B. (2015) *Space vehicle guidance, control, and astrodynamics.* AIAA, Inc, Reston, VA.

Yang, H., Bai, X., and Baoyin. (2017). "Finite-time control for asteroid hovering and landing via terminal sliding-mode control." *Acta Astronautica.* 132 , 78-89.

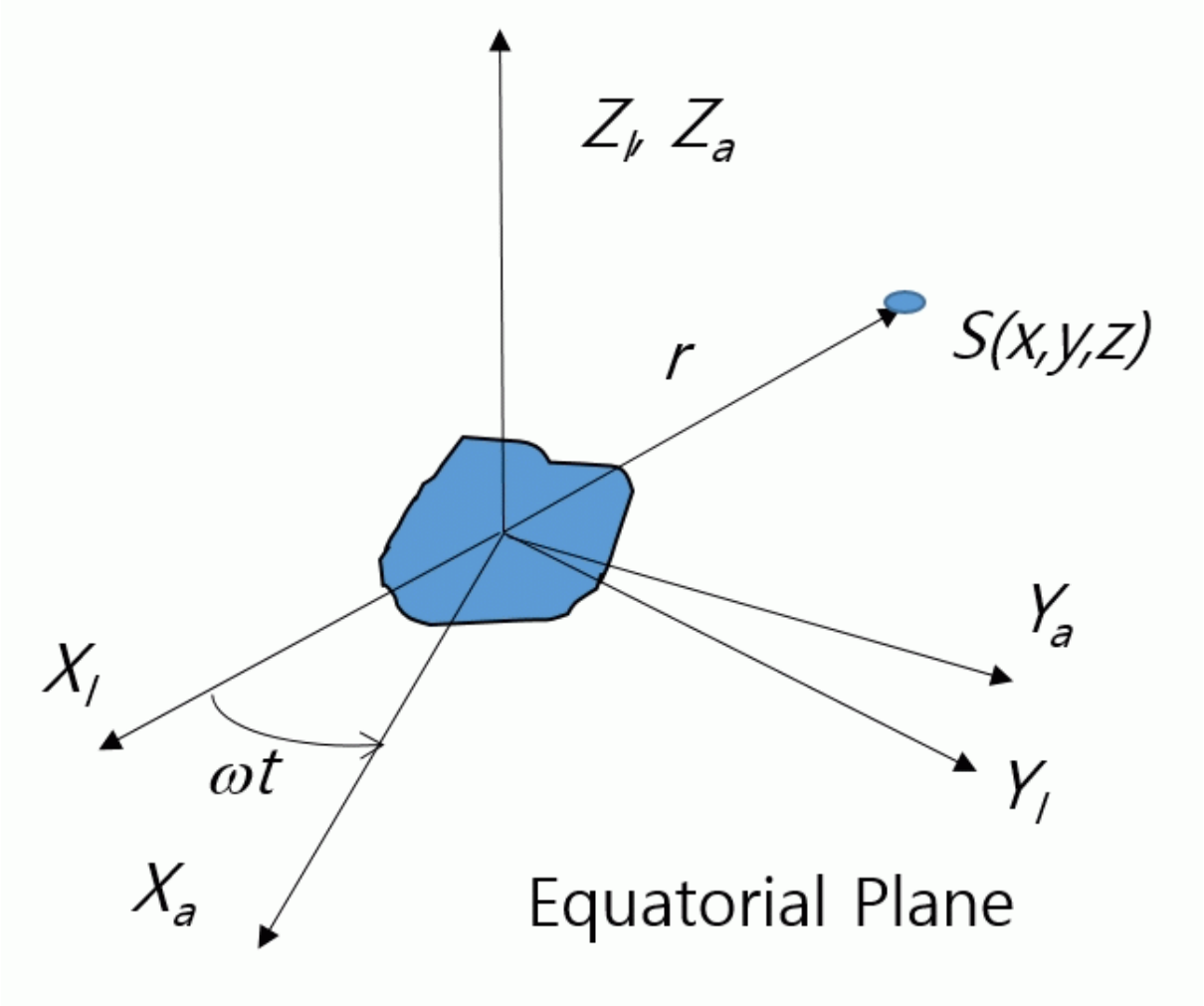

Figure 1: Asteroid coordinate systems

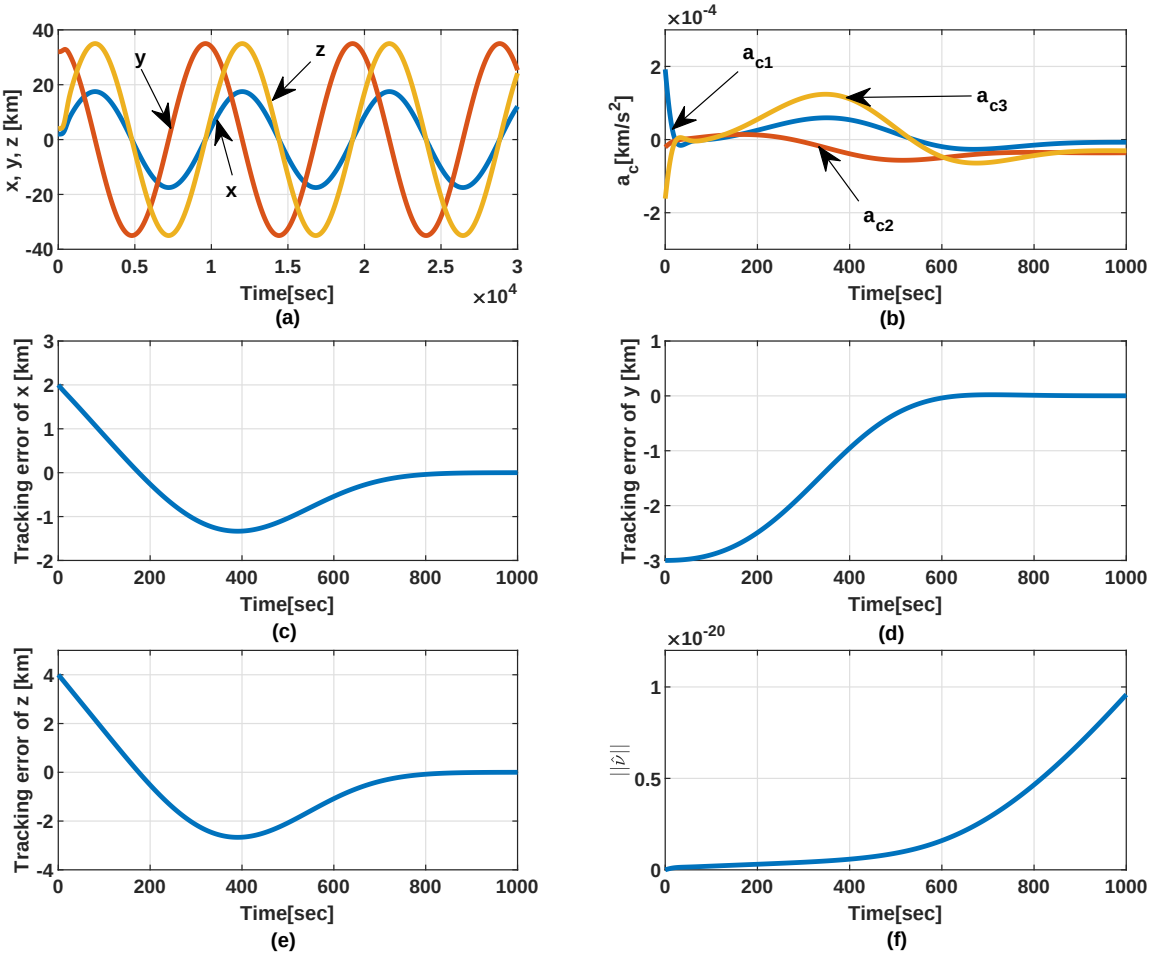

Figure 2: Orbit control around Eros 433 asteroid using adaptive law with command shaping: (a) coordinates (x, y, z); (b) control input $\boldsymbol{a_c}$; (c) x tracking error; (d) y tracking error; (e) z tracking error; (f) parameter estimate norm $||\hat{\boldsymbol{\nu}}||$

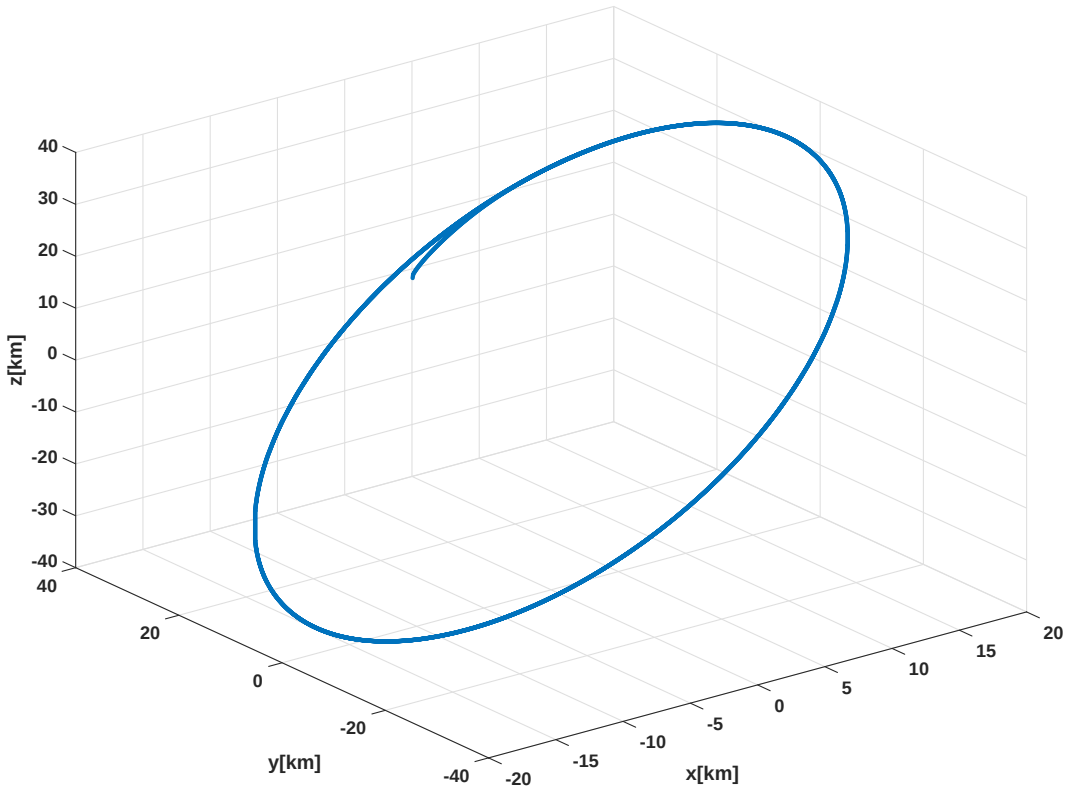

Figure 3: 3-D plot of orbit around Eros 433 asteroid using adaptive law

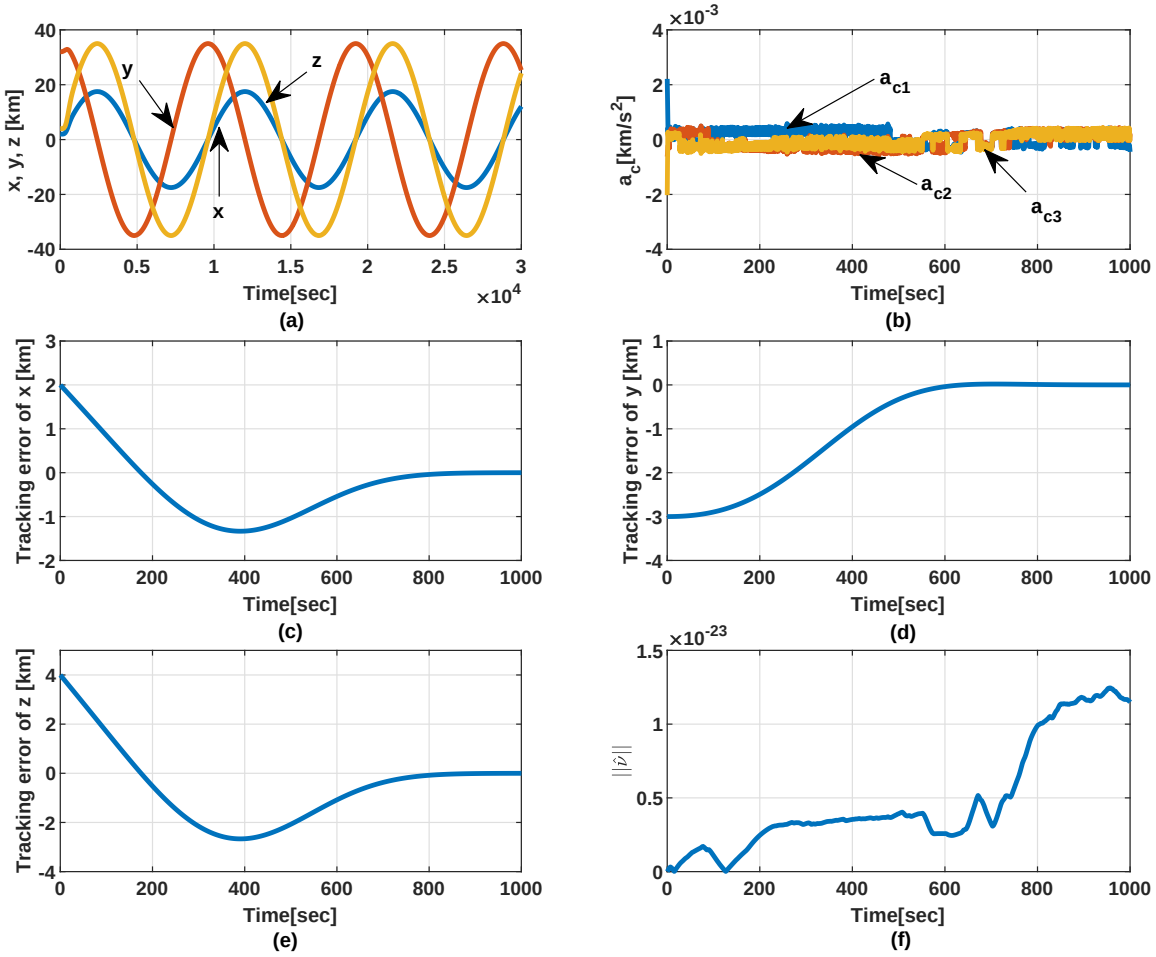

Figure 4: Orbit control around Eros 433 asteroid using STWA law with command shaping: (a) coordinates (x, y, z); (b) control input $\boldsymbol{a_c}$; (c) x tracking error; (d) y tracking error; (e) z tracking error; (f) parameter estimate norm $||\hat{\boldsymbol{\nu}}||$

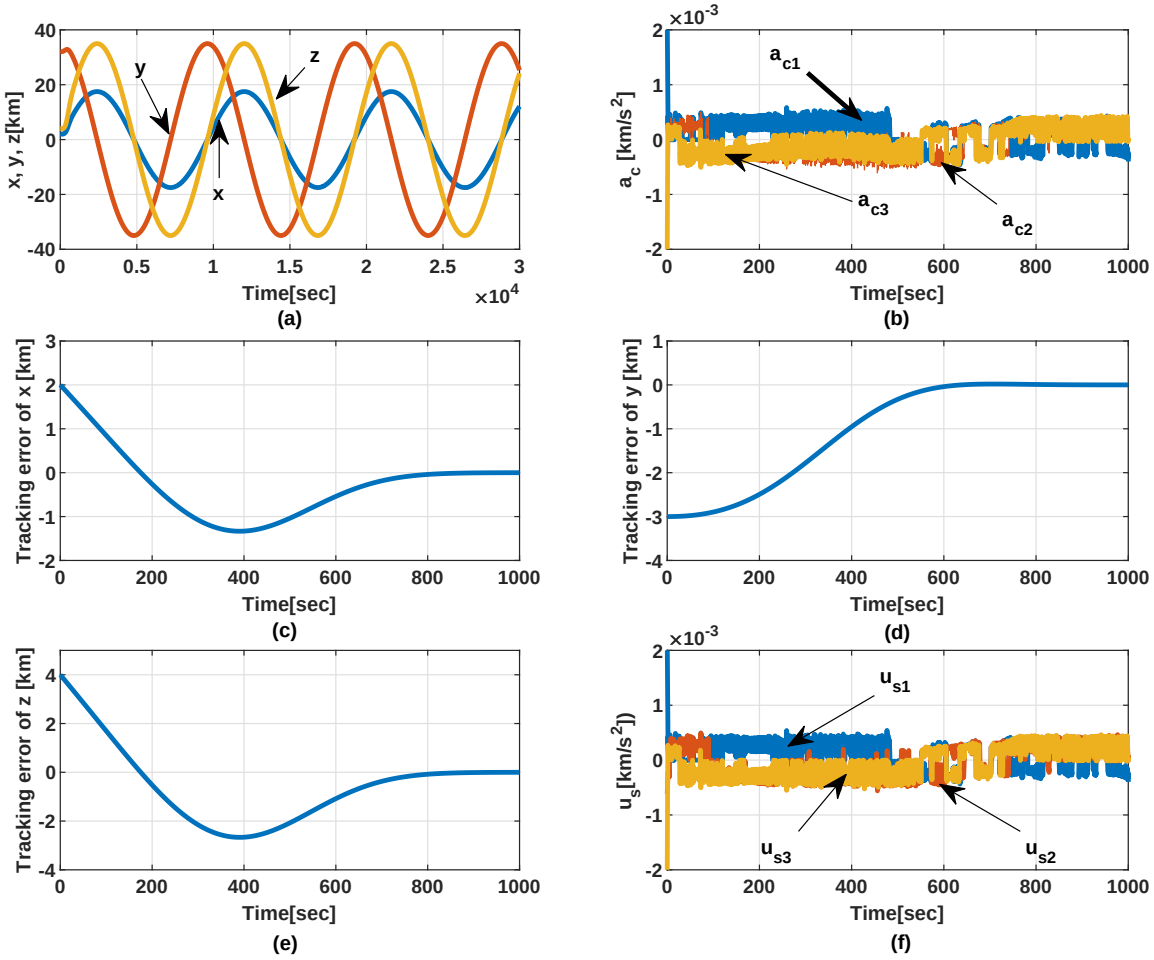

Figure 5: Orbit control around Eros 433 asteroid using STW law with command shaping: (a) coordinates (x, y, z); (b) control input $\boldsymbol{a_c}$; (c) x tracking error; (d) y tracking error; (e) z tracking error; (f) STW law's control input component $\boldsymbol{u_s}$

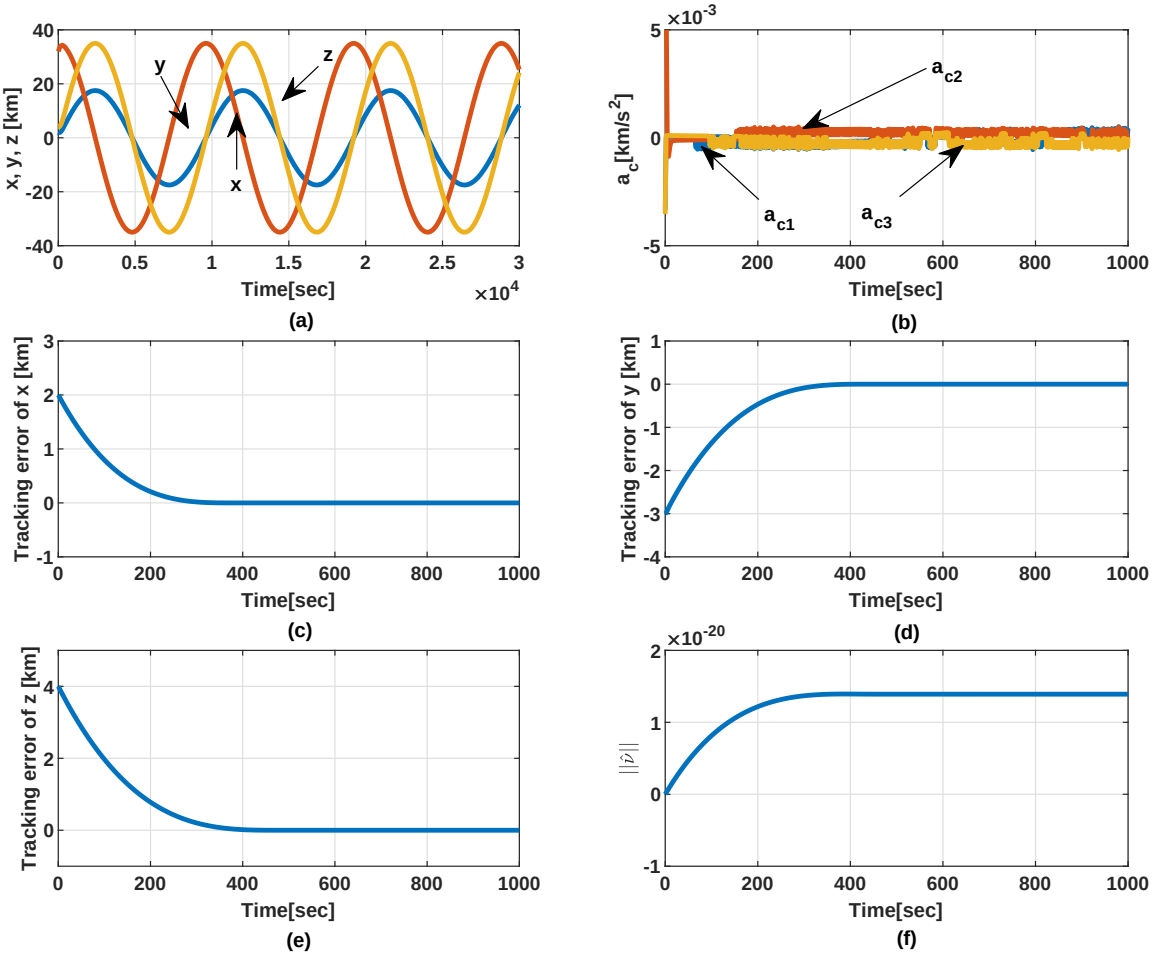

Figure 6: Orbit control around Eros 433 asteroid using STWA law without command shaping: (a) coordinates (x, y, z); (b) control input $\boldsymbol{a_c}$; (c) x tracking error; (d) y tracking error; (e) z tracking error; (f) parameter estimate norm $||\hat{\boldsymbol{\nu}}||$

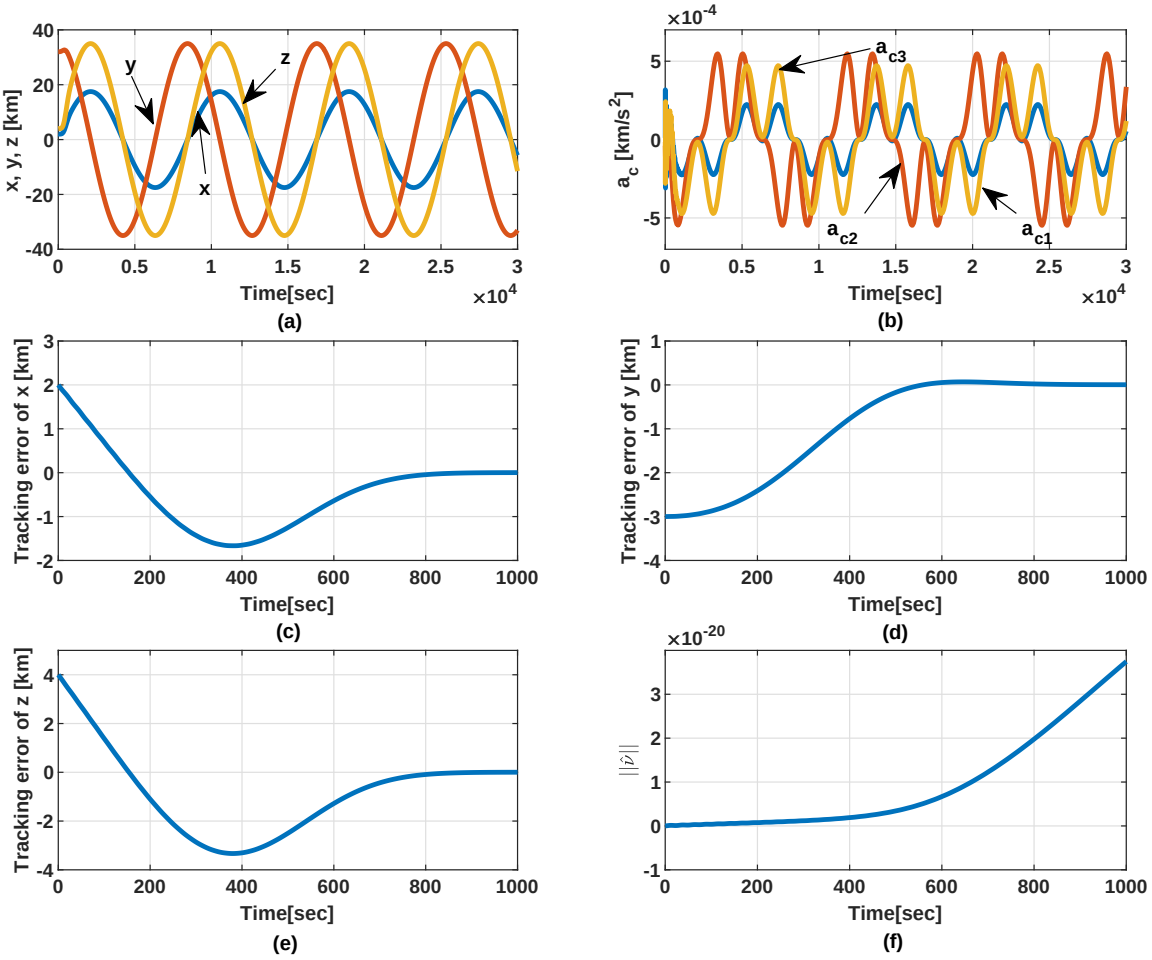

Figure 7: Orbit control around Ida asteroid using adaptive law with command shaping: (a) coordinates (x, y, z); (b) control input $\boldsymbol{a_c}$; (c) x tracking error; (d) y tracking error; (e) z tracking error; (f) parameter estimate norm $||\hat{\boldsymbol{\nu}}||$

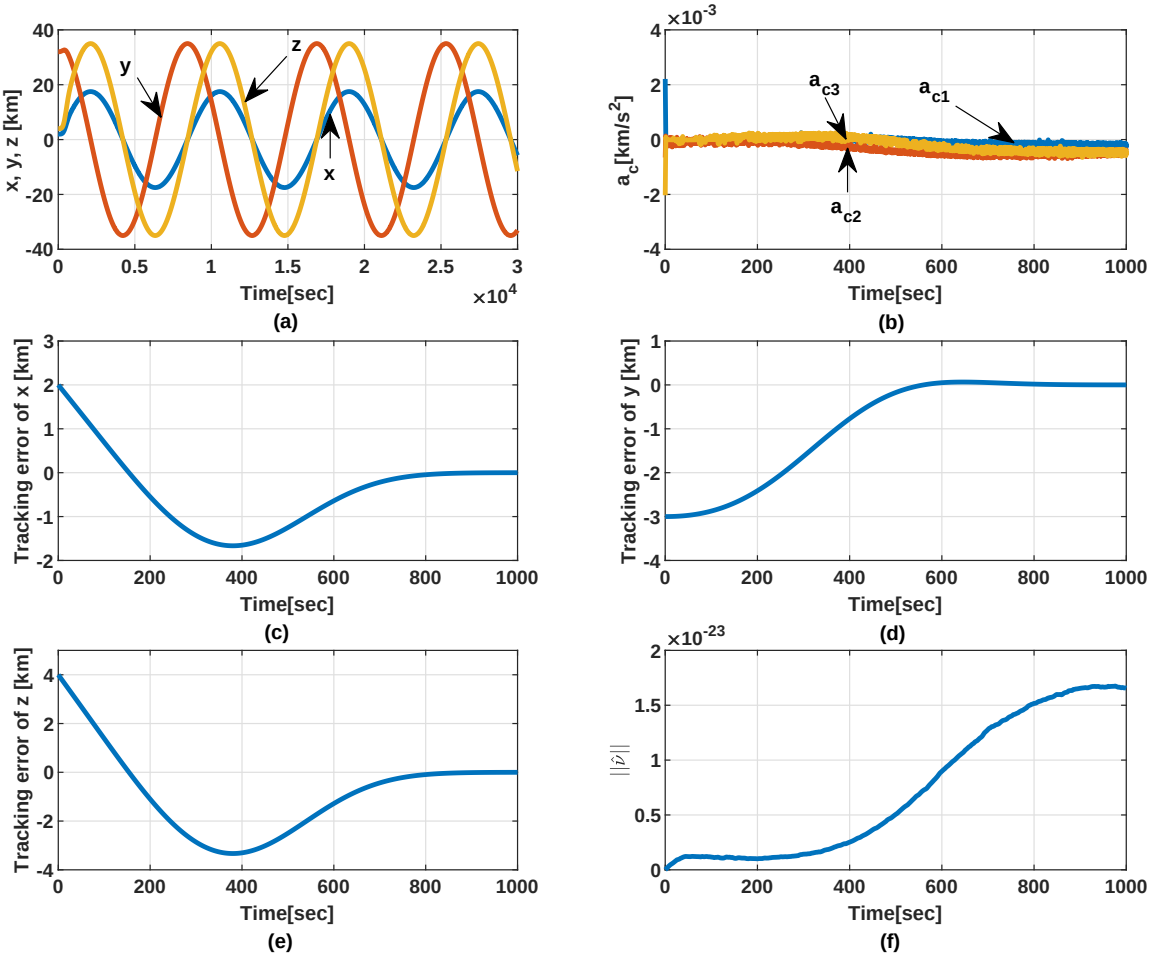

Figure 8: Orbit control around Ida asteroid using STWA law with command shaping: (a) coordinates (x, y, z); (b) control input $\boldsymbol{a_c}$; (c) x tracking error; (d) y tracking error; (e) z tracking error; (f) parameter estimate norm $||\hat{\boldsymbol{\nu}}||$

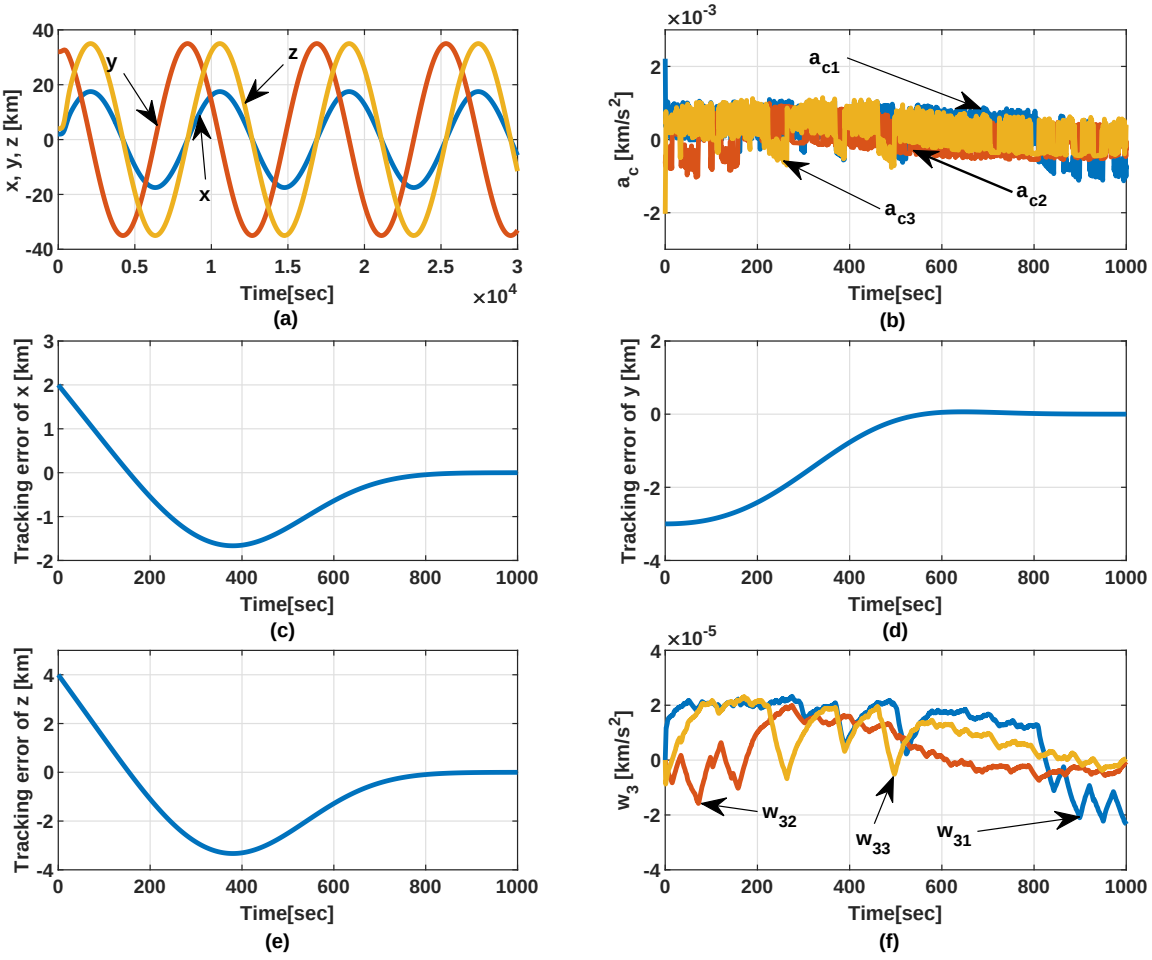

Figure 9: Orbit control around Ida asteroid using STW law with command shaping: (a) coordinates (x, y, z); (b) control input $\boldsymbol{a_c}$; (c) x tracking error,(d) y tracking error; (e) z tracking error; (f) switching function integral control component $\boldsymbol{w_3}$

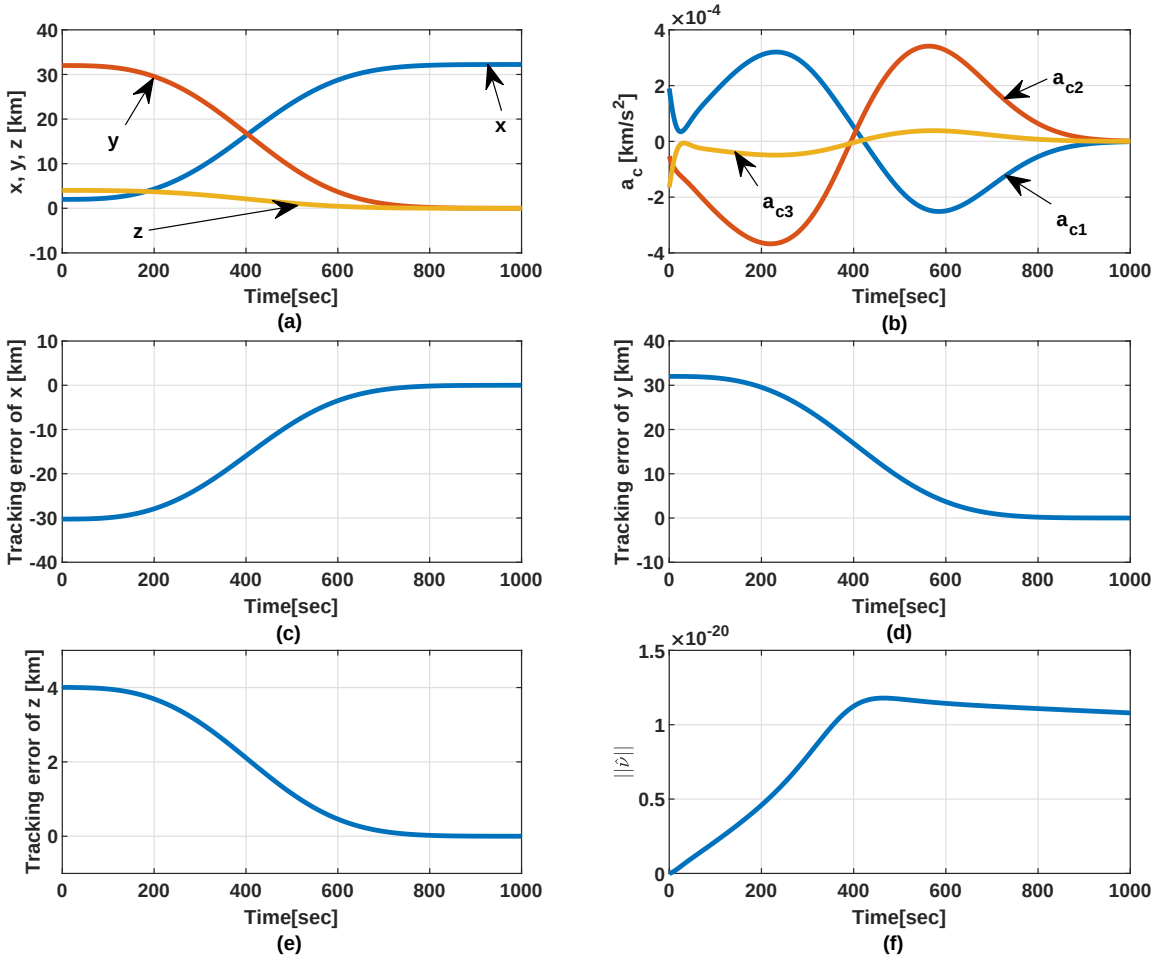

Figure 10: Spacecraft regulation to a fixed point in vicinity of Ida asteroid using the adaptive law with command shaping: (a) coordinates (x, y, z); (b) control input $\boldsymbol{a_c}$; (c) x tracking error; (d) y tracking error; (e) z tracking error; (f) parameter estimate norm $||\hat{\boldsymbol{\nu}}||$